UNIVERSITY OF CRETE

Degree Thesis

X-ray variability study in AGN

Karakonstantakis Angelos A.M. 4515

Supervisor: Prof. Papadakis Iosif

SCHOOL OF SCIENCES & ENGINEERING

Department of Physics

Heraklion, July 2020

Acknowledgments

I would like to express my gratitude to my supervisor Prof. Iosif Papadakis for his guidance in every step of the process. His persistence in detail, allowed me to develop all kind of skills that I will find useful from this point forward to my future.

Table of Contents

CHAPTER 1: Introduction

1.1) Active Galactic Nuclei

*Active Galactic Nucleus (*AGN*)* is a galaxy nucleus which emits an enormous amount of energy in a tiny (astronomically speaking) volume. Their bolometric luminosity can be up to 10^{48} *erg/s* which makes them the most powerful non-explosive sources in the universe. For comparison the solar luminosity is $4\times10^{33} erg/s$.

The AGNs emission varies on short timescales. Especially in X-rays, it can vary on timescales as short as a few hours or even minutes. The observed variability place a constrain to the size of the AGN. Due to causality arguments, there should be a relation between the maximum size of the source, *R*, and its variability timescale, Δt, of the form: $R \approx c\,\Delta t$. Therefore, for a variability time scale of a few hours $R \sim 10^{14} cm = 6700\,AU$. An astronomical unit (AU) is the mean distance from earth to the sun.

Active galaxies come in a variety of types, including Seyfert galaxies, quasars, radio galaxies and blazars. These types were discovered separately and at first seemed quite different, but in recent years a unified model has been developed classifying AGNs in different classes considering changes in only a small number of parameters such as orientation and the presence of jets.

About 10% of the galaxies in the nearby universe host an active nucleus. It is possible that every galaxy goes through an active phase in its lifetime at least once. The fact that we observe a small percentage of galaxies in active state could mean that galaxies become active for a short period of its lifetime. Milky way shows evidence of a low level activity which could mean that our galaxy used to be an AGN in the past.

1.2) Basic ingredients of an AGN

There have been evidences that a *supermassive black hole,* with typical mass of 10^6 to 10^{10} solar masses, resides in the center of each galaxy. Most evidence of the existence of *supermassive black holes* come from dynamical signature (other evidence include the observation of relativistic phenomena in the X-ray emission of AGN). If the supermassive BH is accreting material, then an active nucleus appears.

We can easily disprove the idea that luminosities of 10^{48} *erg/s* (this is a typical luminosity for the bright quasars) can be achieved by stellar processes. Following the calculations of Rosswog & Bruggen (2007), $8\cdot10^5$ O-type stars would be required to produce the luminosity of a AGN. *But, they would have to be located* in a region of ~ 10 light days (which is a typical size of the optical emission region in AGN). This would imply stellar densities of 10^{12} pc^{-3}. Such high densities would lead to frequent collisions and an expedient collapse of the system. Another possibility would be the the case of many supernova explosions. Approximately 10^4 supernovae shinning constantly at their peak luminosity would be required to produce luminosities of 10^{48} *erg/s*. This would required the formation of 10^{10} stars that are permanently producing supernova and, as we mentioned above, such high densities would make the system unstable.

According to the current working model AGNs are powered by material which is accreted to the BH, in the form of a disc. A form of friction (viscosity) acts between neighboring disc rings and material will loose angular momentum. As a result, part of the gas will fall inwards to smaller radius orbits. In doing so, it releases gravitational potential energy, and the disc heats up.

The disc temperature increases towards the center. The amount of energy it is released can be up to *10%* or the particle's rest mass energy. The accretion disc emits as a black body, and this process can explain the optical/UV emission of AGN.

1.3) The AGN emitted spectrum

AGNs emit radiation over the whole spectrum of electromagnetic radiation. The emission in different spectral bands is produced by different radiative mechanisms. For example, the infrared band emission is due to emission from hot, dusty material, located far away from the center, which absorbs light emitted from the central source. The optical and ultraviolet band is due to the emission from the accretion disk. X-rays are produced in a hot plasma, via inverse Compton scattering process. Finally, γ-rays are detected from the so-called "radio-loud" AGN and are emitted from jets of particles that move with relativistic speed.

Figure 1 shows the spectrum from a typical AGN, namely a galaxy called Mrk 509. The observed data are marked with the black crosses (lines of various colors and the solid dark line show the emission of various model components and the overall best-fit theoretical model). At low energies (*<1e-3 keV*) we observe the disc blackbody radiation, the so-called *big blue bump*. Photons emitted by the disc are upscattered to higher energies (X-ray) via Inverse Compton scattering. The spectrum in high energies has a power-law shape up to a cut-off energy, of the order of *~200keV* in this object. This cut-off energy is though to be representative of the electron temperature in the hot plasma that comptonizes the soft photons.

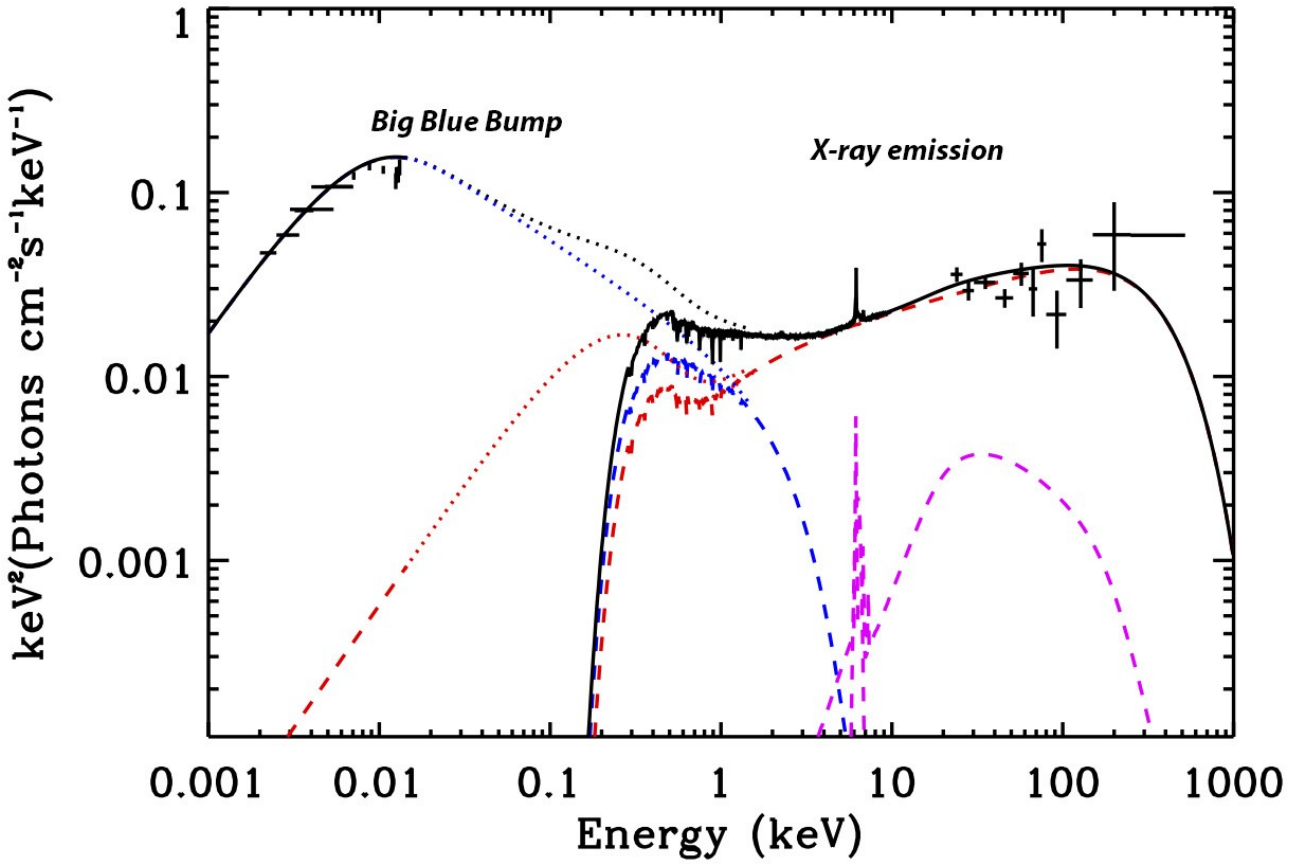

***Figure 1**: A typical AGN spectrum in units of keV for the photon's energy and keV $s^{-1}cm^{-2}$ for the flux (Petrucci et al., 2013).*

1.3.1 The X-ray spectrum of AGN

We will focus to the study of the X-ray emission in AGN. According to the current paradigm, electrons are heated in a region (which is called “corona”). Photons injected in the corona interact with the electrons and are upscattered to higher energies by Inverse Compton scattering. The primary X-ray emission is characterized by a power-law spectra shape extended to energies determined by the temperature of the corona.

The top panel in Fig. 2 shows a distribution of the spectral slope, Γ, of radio-quiet, Type 1 AGN (where we can see the nucleus directly, without any absorption). This figure is from Ricci et al. (2017; Γ is the slope of the spectrum in units of *photons* $s^{-1}cm^{-2}keV^{-1}$). These authors studied hundreds of AGN with *Swift*/BAT and, according of their results, the median value of the photon index in AGN is Γ~2.

As for the cut-off energy, Tortosa et al. (2018) measured the cut-off energy of 19 AGN, using *NuSTAR* data, and they found that most objects have a cut-off energy of *100-200keV*. The distributions of the high energy cut-off of the sample is given in Fig. 3. The high cut-off energy was measured in 12 sources (shown in red), while only a lower-limit was measured in 7 other objects.

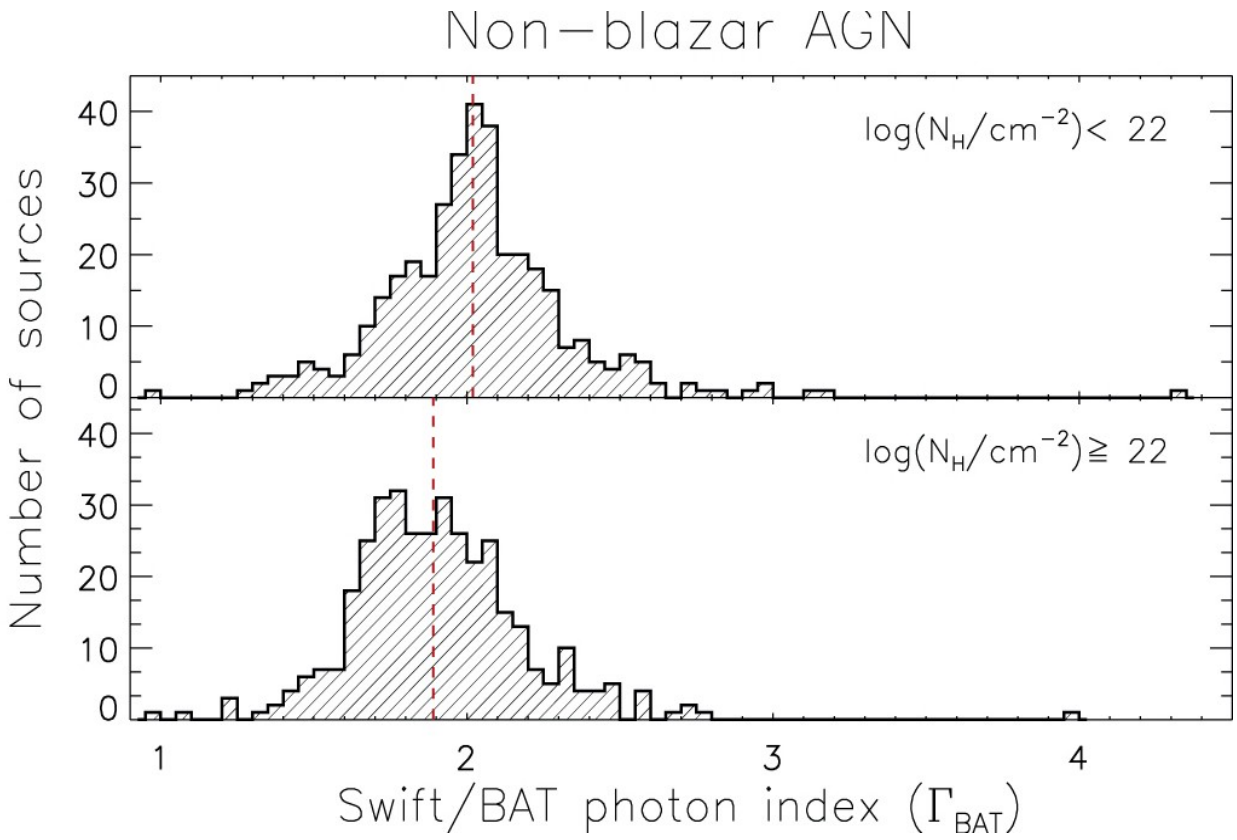

Figure 2: *The distribution of the the photon index, Γ, in AGN (from Ricci et al. 2017).*

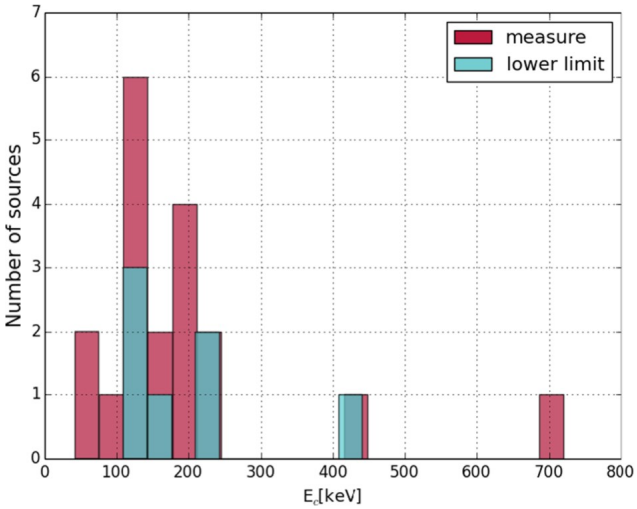

Figure 3: *Distribution of the high energy cut-off energy in AGN (from Tortosa et al., 2018).*

1.3.2 Correlated X-ray flux and spectral variability in AGN

X-ray emission in AGN is highly variable. In many objects we observe variations of the order of a few over time scales as short as one hour. The sources vary both in flux and in spectral shape.

Sobolewska & Papadakis (2009) studied the X-ray variability of 10 different AGN over a long period of time (~7-11 years). They found that Γ increases as flux increases in almost all sources.

As an example, Fig. 4 shows the X-ray spectra slope vs X-ray flux plot int he case of the Type 1 AGN NGC 4051. Clearly, the spectrum becomes steeper (i.e. the spectral slope, Γ, increases) as the flux increases. The results for the other AGN studied by Sobolewska & Papadakis (2009) show a similar behavior.

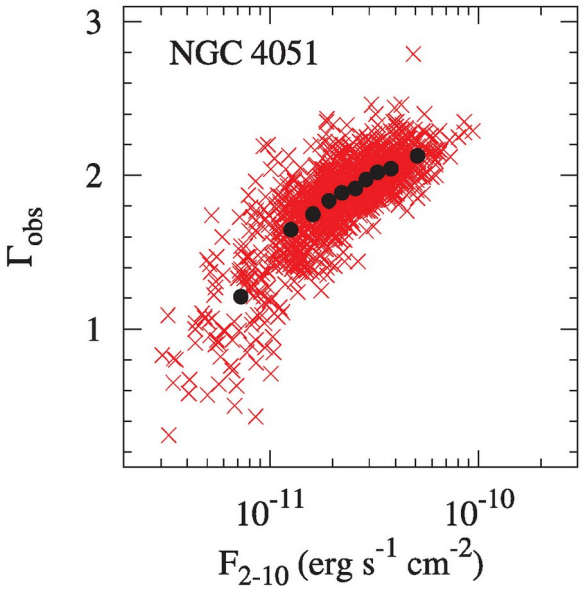

Figure 4: *The relation between Γ and 2-10keV flux in NGC4051 (from Sobolewska & Papadakis 2009).*

1.3.3 The correlation of the X-ray flux in different energy bands

The variations that are observed in AGN are very similar, across the full X-ray band (which is usually the band between 0.5-10 keV). Most of times, we observe the same variations is the soft (i.e. below 2 keV) and hard band (i.e. at energies above 2 keV), but with a delay.

Figure 5 shows the light curve of NGC 4051, as observed with EXOSAT, in the low energy band (LE: 0.05-2 keV) and high energy band (ME: 2-10 keV). The light curves in this figure are normalized to their mean. The correlation between the LE (thin line) and the ME (bold line) light curves is almost perfect. The variations are of the same amplitude, but the LE light curves decrease faster than the light curves in the ME and this pattern is repeated. In addition, the peak of the flux

appears slightly delayed in the ME band. Therefore, there is a delay between the variations in the softer band with respect to the variations in the higher energy band, with the latter being delayed with respect to the former.

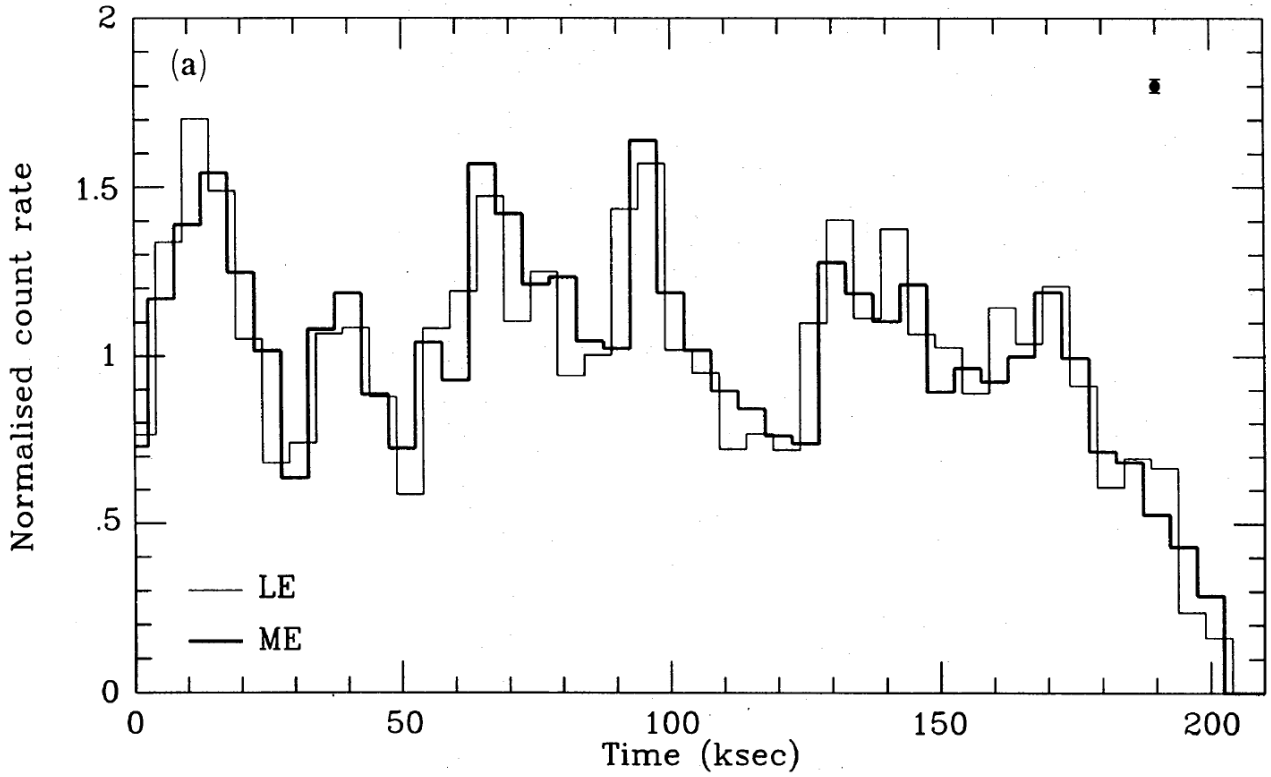

Figure 5: *X-ray Light curves of a low energy band (thin line) and a medium energy band (bold line). Light curves are normalized to their average value (from Papadakis & Lawrence 1995).*

1.4) The main objective of this works

The main goal of this work is to study the origin of the X-ray variability in AGN. To achieve this, we we will study a specific model that was proposed by Galeev, Rosner, & Vaiana (1979), as was later modified by Haardt et al. (1994). The basic idea of the model is that accretion disc is magnetized. Because of the differential rotation, the magnetic field is amplified, giving rise to loop-like magnetic flux tubes which emerge, via buoyancy, above the disc.

The magnetic field essentially provides an energy source for plasma heating in these loops, which contain very hot plasma. Low energy photons from the underlying disc, enter the corona and hard X-ray emission is the consequently result, since the photos interact with the plasma particle and scattered to higher energies via comptonization. Figure 6 shows the model picture, with the active regions (or: “blobs”) distributed above the disc. According to the model, the are the X-ray corona above the disc, which produces the X-rays.

The main objective of the work of this work is to study the expected spectral evolution of the emission from these regions, and compare the theoretical results with the observations.

We discuss the concept of computerization is the following Chapter as well as the model of Galeev, Rosner, & Vaiana (1979) in detail in Chapter 3. In Chapter 4, we consider an exponential decay of the corona luminosity characterized by a discharge time scale. By doing this we try to simulate the time evolution of a single loop-like structure which we call “blobs”.

To compute the spectrum of this blob we use a comptonization code, called EQPAIR (Coppi, 2002). In Chapter 4, we analyze the results produced by EQPAIR and we compare the spectral evolution with the expected observational values we discussed in this Chapter. The main result is that the proposed model, under the assumptions we considered cannot explain the observational results from the X-ray studies of AGN.

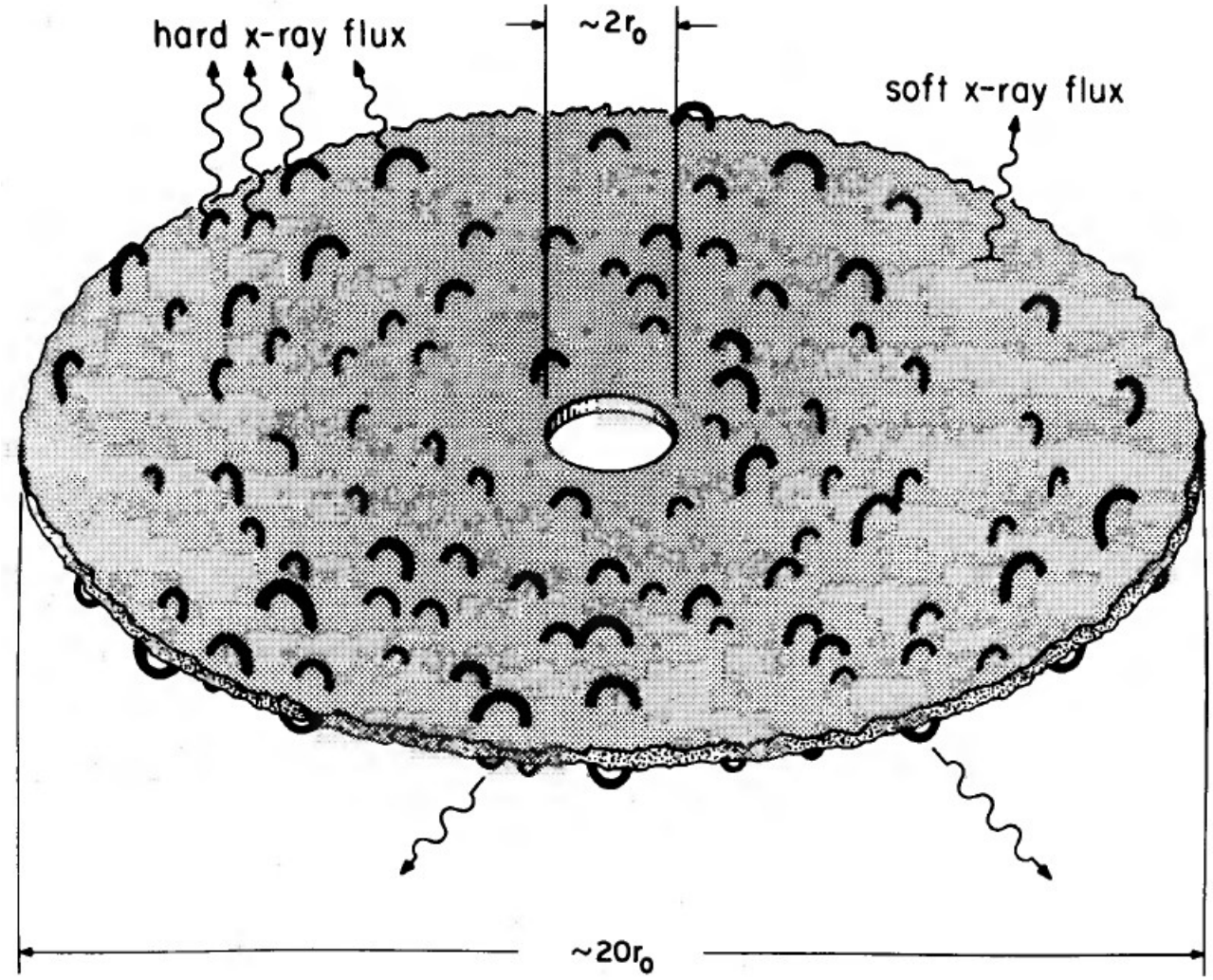

Figure 6: *A schematic drawing of the Galeev, Rosner, & Vaiana (1979) model of X-ray emission in AGNs.* $r_o = 6GM/c^2$ *which is the last stable cirtular orbit for a non-rotating black hole. This drawing show how the loop-like structure comptonize the disc photons, producing hard X-ray flux.*

CHAPTER 2: Comptonization

2.1) Compton Scattering

Compton Scattering describes the effect of a photon losing energy by interacting with an electron. We consider an electron at rest and an incoming (incident) photon of energy $\mathcal{E}$ which becomes $\mathcal{E}_1$ after scattering (in the laboratory frame). Let us denote with θ the scattering angle between the incoming and the scattered direction (see Fig.7). Conservation of energy and conservation of momentum along the *x* and *y* axis gives (Rybicki & Lightman, 1979):

$$\mathcal{E}_1 = \frac{\mathcal{E}}{1+\frac{\mathcal{E}}{m_e c^2}(1-cos\theta)} . \tag{1}$$

Since $\mathcal{E}=\frac{hc}{\lambda}$ then, $\frac{hc}{\lambda_1}=\frac{hc/\lambda}{1+\frac{hc/\lambda}{m_e c^2}(1-cos\theta)} \Rightarrow \lambda_1-\lambda=\frac{h}{m_e c}(1-cos\theta)$. The quantity $h/m_e c$ is known as Compton wavelength (λ_c) and it is equal to $\lambda_c \equiv \frac{h}{m_e c}=0.02426\ \AA$. Thus, eq.(1) can be written as:

$$\lambda_1-\lambda=\lambda_c(1-cos\theta) . \tag{2}$$

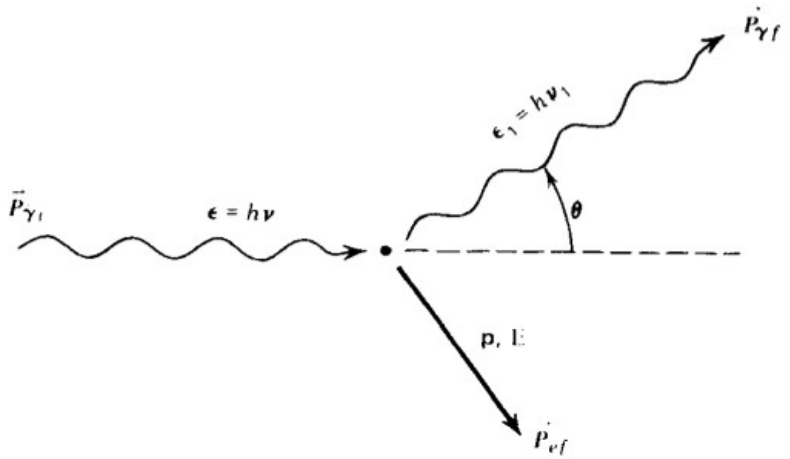

***Figure 7**: Geometry of Compton scattering adapted from Rybicki & Lightman, 1979*

2.2) Inverse Compton Scattering

In the previous section we described the direct Compton process where energy is transferred from the photons to the electrons. The opposite process is called Inverse Compton scattering: the electron energy is greater than the typical photon energy and there can be energy transfer from the electron to the photon. Since, X-rays in AGN may be produced by Inverse Compton scattering of photons emitted by the accretion disc by hot and energetic electrons located in a "corona" lying above the accretion disc, we will examine this process in more detail.

First we will investigate the importance of Inverse Compton scattering in case of photons scattered repeatedly through a medium of energetic electrons. The main parameter that determines the importance of the Inverse Compton scattering is the so-called "Compton parameter *y"*, which is defined as:

$$y=\left\{\frac{\text{average fractional energy change}}{\text{per scattering}}\right\}\times\left(\frac{\text{mean number}}{\text{of scatterings}}\right). \tag{3}$$

When $y\geqslant 1$ the total photon energy and spectrum will be significantly changed and the Comptonization process is important. To get an estimate of *y*, first we will estimate the average fractional energy change per scattering (first term in the right hand side of the equation above). Then we will estimate the mean number of scatterings which is the second term in the right hand side of the above equation.

2.2.1 Average fractional energy change

Let us assume that the electrons follow a non-relativistic *Maxwellian thermal distribution* with temperature T_e. In general photons gain or lose energy as they interact with the electrons. It can be shown that (Rybicki & Lightman, 1979)

$$\frac{\Delta\mathcal{E}}{\mathcal{E}}=\frac{\mathcal{E}_1-\mathcal{E}}{\mathcal{E}}=-\frac{\mathcal{E}}{m_e c^2}+a\frac{kT_e}{m_e c^2}. \tag{4}$$

The first term of the equation above, $-\mathcal{E}/(m_e c^2)$, is the energy lost in scattering and the second term, $akT_e/(m_e c^2)$, is the energy gain by photons, where *a* is a coefficient to be determined.

To estimate *a*, we consider the case when photons and electrons are in equilibrium meaning that on average, energy gains equal losses (i.e. $\langle\Delta\mathcal{E}\rangle=\langle\mathcal{E}_1\rangle-\langle\mathcal{E}\rangle=0$). We consider only scattering, neglecting absorption. In this case, it can be shown (Rybicki & Lightman, 1979):

$$\langle\mathcal{E}\rangle=3kT_e, \tag{5}$$

$$\langle\mathcal{E}^2\rangle=12(kT_e)^2. \tag{6}$$

Multiplying eq.(4) with $\mathcal{E}$, we get $\Delta\mathcal{E}=-\frac{\mathcal{E}^2}{m_e c^2}+a\frac{kT_e}{m_e c^2}\mathcal{E}$. Since we are at equilibrium and $\langle\Delta\mathcal{E}\rangle=0$, we will get the following:

$$a\frac{kT_e}{m_e c^2}\langle\mathcal{E}\rangle-\frac{\langle\mathcal{E}^2\rangle}{m_e c^2}=0\Rightarrow\frac{3kT_e}{m_e c^2}(a-4)kT_e=0\Rightarrow a=4.$$

Now eq.(4) becomes,

$$\Delta\mathcal{E}=\frac{\mathcal{E}}{m_e c^2}(4kT_e-\mathcal{E}). \tag{7}$$

In the case when $4kT_e>\mathcal{E}$ energy is transferred from electrons to photos (i.e. the case of Invert Compton scattering). In the case where $4kT_e\gg\mathcal{E}$ the average fractional energy increase per collision should be,

$$\frac{\Delta\mathcal{E}}{\mathcal{E}}\simeq\frac{4kT_e}{m_e c^2}. \tag{8}$$

2.2.2 Mean number of scatterings

So far we have estimated the average fraction energy per scattering, the first term in the right hand side of eq.(3). Now, we will estimate the second term of the equation, the mean number of scatterings *N*.

We assume a region of size *R*, with electrons that have a temperature of T_e, and a numerical density of N_e. The optical depth for scattering will be equal to $\tau = N_e \sigma_T R$, where σ_T is the Thomson cross section. Consider a photon traveling in the medium. In the case $\tau \simeq 1$ or smaller, when the photon travels a distance *R* (the size of the medium), it will interact with an electron of cross-section σ_T if electron exists in the volume $\sigma_T R$. The average number of electrons in this volume, which means the average number of scatterings, is $N = N_e \sigma_T R$, which is equal to τ.

For regions of large optical depth a photon will be scattered many times before leaving the medium, at random directions. In this case the average number of scattering is not equal to τ. To estimate the mean number of scattering in this case, we assume isotropic scattering, which means that the photos has equal probability to be emitted to any angle after scattering. Let us follow a photon which enters the scattering region and travels a displacement $\vec{r}_1$ before being scattered. Then it travels a new direction displacement $\vec{r}_2$ before being scattered for the second time, and so on. The displacement of the photon after *N* scatterings is $\vec{R} = \vec{r}_1 + \vec{r}_2 + \vec{r}_3 + \cdots + \vec{r}_N$. The mean square displacement traveled by photons will be

$$\vec{l}_*^{\,2} = \langle \vec{R}^2 \rangle = \langle \vec{r}_1^{\,2} \rangle + \langle \vec{r}_2^{\,2} \rangle + \langle \vec{r}_3^{\,2} \rangle + \cdots + \langle \vec{r}_N^{\,2} \rangle + 2\langle \vec{r}_1 \cdot \vec{r}_2 \rangle + 2\langle \vec{r}_1 \cdot \vec{r}_3 \rangle + \cdots = Nl^2 \Rightarrow l_* = \sqrt{N}\, l \,, \tag{9}$$

where $l = (N_e \sigma_T)^{-1}$ is the mean free path of photon. The cross terms in the equation above involve averaging the cosine of the angle between $\vec{r}_i$ and $\vec{r}_j$, which is 0 for isotropic scattering. When the photons exit the medium, $l_* \sim R$, the typical size of the medium. And from eq.(9) $N \approx \frac{l_*^2}{l^2} = \frac{R^2}{l^2} = \frac{\left[\tau \cdot (N_e \sigma_T)^{-1}\right]^2}{\left[(N_e \sigma_T)^{-1}\right]^2} = \tau^2$. Therefore, $N \approx \tau^2$, *τ»1*. For most estimates it is sufficient to use $N \approx \tau^2 + \tau$ or

$$N \approx max(\tau, \tau^2) \,. \tag{10}$$

Thus, the second term in eq.(3) is $max(\tau,\tau^2)$.

2.2.3 Compton parameter *y*

Combining the equations 3, 8 and 10 we obtain the expression of the Compton *y* parameter:

$$y = \frac{4kT_e}{m_e c^2} max(\tau, \tau^2) \,. \tag{11}$$

For the comptonization possess to be important ($y \gg 1$) the mean electron temperature, which determines the average photon energy change per scattering and/or the optical depth should be high.

2.3) Comptonization Spectra

In this section, we will discuss the spectra produced by repeated Compton scattering of photos by thermal electrons with $4kT_e \gg \mathcal{E}$. We will discuss the case of a medium of non relativistic thermal electrons with optical depth *τ≥1*.

We have already show in eq.(8) that the mean energy gain after each scattering, when $4kT_e \gg \mathcal{E}$, is $4kT_e/m_e c^2$ or

$$\frac{\mathcal{E}_1}{\mathcal{E}} = 1 + \frac{4kT_e}{m_e c^2} . \tag{12}$$

Therefore after *K* scatterings, the final photon energy will be:

$$\frac{\mathcal{E}_K}{\mathcal{E}} = \left(1 + \frac{4kT_e}{m_e c^2}\right)^K . \tag{13}$$

Since $4kT_e \ll m_e c^2$ we can make the approximation $\left(1 + \frac{4kT_e}{m_e c^2}\right) \approx \exp\left(\frac{4kT_e}{m_e c^2}\right)$, therefore,

$$\frac{\mathcal{E}_K}{\mathcal{E}} = \left(1 + \frac{4kT_e}{m_e c^2}\right)^K = \exp\left(K\frac{4kT_e}{m_e c^2}\right), \tag{14}$$

where *K* is the number of scatterings. We have shown in section 2.2.2 that $K = max(\tau, \tau^2)$. Thus, using eq.(11), the exponential term in eq.(14) is equal to *exp(y)*, hence,

$$\frac{\mathcal{E}_K}{\mathcal{E}} = \exp(y) . \tag{15}$$

To determine the Comptonization spectrum under such conditions we must consider the *Kompaneets equation:*

$$\frac{\partial n}{\partial y} = \frac{1}{x^2}\frac{\partial}{\partial x}\left[x^4\left(n + n^2 + \frac{\partial n}{\partial x}\right)\right], \tag{16}$$

where *x* is the energy in units of kT_e $x = h\nu/kT_e$, *n(x)* is the number of photons of energy *x and y* is the Compton parameter. The solution to *Kompaneets equation* describes the evolution of the photon spectrum due to repeated scattering of photons by non relativistic thermal electrons. The equation can be solved analytically only for special cases and simple geometries. In general cases, it must be solved by numerical integration. For the case of $\tau \geq 1$, the solution for the spectrum intensity up to energies $h\nu \sim kT_e$, has a power-law form (Longair, 1992):

$$I(\nu) \propto \nu^{3+m} , \tag{17}$$

where $m = -\frac{3}{2} \pm \sqrt{\frac{9}{4} + \frac{1}{y}}$ and the Compton parameter *y* is defined by eq.(11). The + root corresponds to $y \gg 1$ and for $y \ll 1$ the - root is appropriate. For $y \sim 1$ we must take a linear combination of of the two solutions. Also note that for $y \gg 1$, *m=0* and $I_{(\nu)} \propto \nu^3$.

Figure 8 shows the Comptonization spectra, in the case of low energy photons in a spherical plasma cloud with a temperature of $kT_e = 25keV$. The spectra have a power-law shape, up to a maximum energy, E_c, which is characteristic of the electron temperature (the vertical dashed line indicates the electrons' temperature, *kTe=25eV*). At higher energies the flux decreases highly exponentially i.e. $\propto e^{-E/E_c}$. Monte Carlo simulations of the Compton process (stepped lines) are compared with the analytical solutions of the *Kompaneets* equation (solid line). In general there is a good agreement between the two.

The figure shows how the spectrum changes as y increases. For large optical depth the spectrum evolves so that the formation of a Wien peak can be observed. For smaller optical depths the spectrum has a power-law shape up to energies of kT_e.

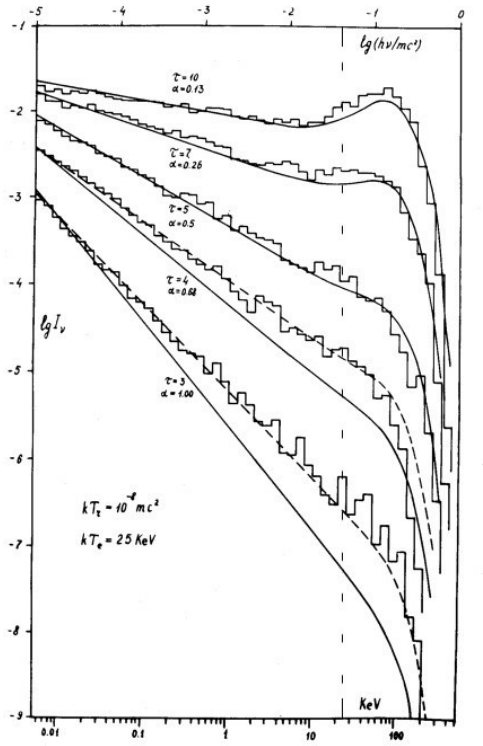

***Figure 8**: The componization of low energy photons in a spherical plasma cloud of temperature $kT_e = 25\,keV$ (taken from Pozdyakov et al. 1983).*

CHAPTER 3: An X-ray variability model

We will study the variability properties of the accretion disc dynamo model of Galeev, Rosner & Vaiana (1979; hereafter GRV), as elaborated by Haardt et al. (1994). In this model a fraction *f* of the total accretion power is stored in magnetic fields, which are assumed to be present in the disc, and the rest *(1-f)* is dissipated in the accretion disc. According to the model, the disc differential rotation leads to an exponential amplification of the azimuthal component of the magnetic field. Magnetic field lines reconnection within the disc is inadequate in preventing the grow of the magnetic field so, the magnetic field is amplified until magnetic pressure equals the surrounded gas pressure. In this case, looplike magnetic flux tubes emerge via buoyancy above the disc.

However magnetic field line reconnection is expected to happen quickly above the disc. When this happens the stored magnetic energy is released and it can heat the electrons in the magnetic structures. Low energy photons produced by the disc will enter those regions and then, photons will be upscattered to higher energies (i.e. X-ray) by inverse Compton scattering. Therefore, these "active regions" will be bright in X-rays. In effect, they will be the X-ray source in these objects, and we will call them hereafter as "X-ray blobs".

3.1) The assumed geometry

We assume an AGN with a non-rotating BH, with a mass of $10^7 M_\odot$, and an X-ray luminosity which is $\sim 10\%$ of the bolometric luminosity, as it is usually observed (e.g. Lusso, 2012). The observed optical/UV luminosity in typical AGN corresponds to luminosities which imply a mass accretion rate of *~5%* of the Eddington limit[1]. Since the power necessary for both X-ray and disc luminosity is provided by the accretion process, We will assume a total accretion power of *5.5%* of Eddington's limit (i.e. $\dot{M}/\dot{M}_{Edd}=0.055$). Out of this accretion power 0.5% will be stored to magnetic field and is given to heat electrons, and then to X-rays, and the rest 5% will account for the disc emission. Therefore,

$$f=\frac{(accretion\ power\ for\ \text{X-rays})}{(total\ accretion\ power)}=\frac{0.005\,L_{Edd}}{0.055\,L_{Edd}}\approx 0.09\ . \qquad (18)$$

We will also consider blobs that are located at a distance $R_d=10R_g$[2], where the X-ray emissivity is maximum (Haardt et al., 1994). The size of the X-ray emitting region (i.e. of the X-ray blob), according to GRV, is given by

$$R_b=z_0/a^{1/3}\ , \qquad (19)$$

where z_0 is the disc scale height and a is the disc viscosity. According to Svensson & Zdziarski (1994), when $f=0.09$ and $\dot{M}/\dot{M}_{Edd}=0.055$, radiation pressure exceeds gas pressure at $R=10R_g$. In this case the scale height z_0 at a distance R is given by

---

1 This is equal to the accretion rate necessary for the disc's luminosity to be equal to the Eddington luminosity, which is defined as: $L_{Edd}=\frac{4\pi G M_{BH} m_{proton} c}{\sigma_T}$, where G is the gravitational constant, M_{BH} is the central mass, m_{proton} is the proton mass, c the speed of light and σ_T is the Thomson cross section. Assuming an efficiency rate of $\varepsilon=0.1$, then $M_{Edd}=L_{Edd}/(\varepsilon c^2)$.

2 R_g is the gravitational radius of the BH, defined as: $R_g=GM_{BH}/c^2$. For a BH of mass $M_{BH}=10^7 M_\odot$, $R_g=1.5\cdot 10^{12} cm$.

$$z_0 = \frac{3}{4}\left(\frac{\dot{M}}{\dot{M}_{Edd}}\right) S(R)(1-f) R_g \,, \tag{20}$$

where $S(R) = 1 - \left(6\, R_g / R\right)^{1/2}$. Then, at a distance $R = R_d = 10R_g$, for $\dot{M}/\dot{M}_{edd} = 0.055$, $f = 0.09$ and $a = 0.1$, using eq.(19) and eq.(20), we get

$$R_b = z_0 / a^{1/3} = 0.019\, R_g = 0.019 \cdot 1.5\text{e}12\, cm = 3 \cdot 10^{10}\, cm \,. \tag{21}$$

Based on what we have discussed so far, the geometry of the system will be like the one shown in Fig. 9. A spherical hot corona of radius R_b is lying above the surface of the accretion disc at a distance $R_d = 10R_g$. R_{in} is the inner radius of the disc, which is equal to $6R_g$ (this is the radius of the last stable orbit in the case of non-rotating black hole).

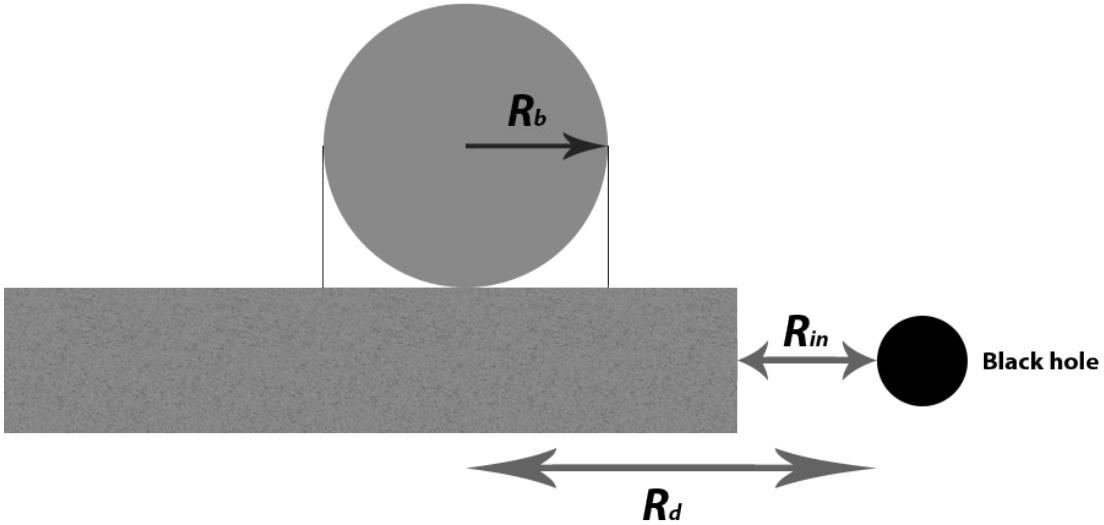

Figure. 9: A sketch of the model geometry. For clarity reasons the image is not in scale.

According to (Haardt et al., 1994) the luminosity of a single blob located at distance R is

$$L_{blob}(R) = 1.7 \cdot 10^{44} \left(\frac{M}{10^7 M_\odot}\right)\left(\frac{f}{0.2}\right)\left(\frac{\alpha}{10}\right)\left(\frac{0.1}{a}\right)^{2/3}\left(\frac{R}{R_g}\right)^{-1/2}\left(\frac{\dot{M}}{\dot{M}_{edd}}\right) S(R)\, erg/s \,, \tag{22}$$

where α is a constant which has been estimated to be *~10* by observations of solar flares (Haardt et al., 1994). In our case, for the values we have assumed ($M = 10^7 M_\odot$, *f=0.09*, *a=0.1*, $R = 10R_g$ $\dot{M}/\dot{M}_{edd} = 0.055$),

$$L_{blob} = 3 \cdot 10^{41}\, erg/s \,. \tag{23}$$

This is the power that is released by the magnetic field, and is used to heat the electrons and power the X-ray emission of the source. Photons produced by the disc, enter the blob. The blob itself is filled with electrons which are heated by the magnetic field and they will upscatter the soft disc photons to higher energies producing the X-ray spectrum via Comptonization. In order to calculate the X-ray spectrum emitted by the blobs, we will use `EQPAIR`, which is a publicly available componization code.

3.2) EQPAIR

The EQPAIR code (Coppi, 2002), is incorporated into the standard X-ray analysis software XSPEC. The code assumes a spherical cloud with isotropic and homogeneous distribution of photons and electrons. Soft, seed photons, are supposed to be distributed uniformly within the plasma. In our calculations we have considered a purely thermal distribution of electrons (i.e. Maxwellian) but EQPAIR is capable of producing the emission from a non thermal distribution of particles and even from a combination of a Maxwellian distribution with a power law tail (hybrid distribution). The main physical radiative mechanism of the model is inverse Compton scattering, but EQPAIR also considers pair production, bremsstrahlung and Coulomb thermalization.

The code is generally used for spectral fitting to obtain the physical parameters of a source but we have used EQPAIR to produce theoretical model spectra, determined by given parameters, with the aim to study the temporal evolution of the emitted luminosity in various energy bands, under different variability scenarios.

As we have shown in section 2.2, the parameter that determines whether inverse Compton scattering is important, or not, is the Compton *y* parameter which depends on the electrons' optical depth and the plasma temperature. The optical depth of the electrons, τ_p, is a free parameter of the model. The temperature is calculated self-consistently by the code by taking into account the power heating the electrons, the luminosity of the soft photons, and τ_p.

The input luminosities are given in terms of the so-called compactness parameter, *l*. The compactness of a region of radius *R*, filled with photons with luminosity *L*, is defined as follows:

$$l = \frac{L}{R}\frac{\sigma_T}{m_e c^3}, \tag{24}$$

where σ_T is the Thomson cross section, m_e the electron mass and *c* the speed of light. The compactness parameter is dimensionless. In our case, L_{blob} (see eq.22) is the "heating rate" (i.e. the power) that is given to electrons by the magnetic reconnection process. This is also the luminosity of the X-ray photons will be produced by the hot plasma via Comptonization and we will observe. We therefore define the X-ray compactness of the source as:

$$l_h = \frac{L_{blob}}{R_b}\frac{\sigma_T}{m_e c^3}. \tag{25}$$

In the same way, we can also define the compactness of the soft photons in the corona, as:

$$l_s = \frac{L_s}{R_b}\frac{\sigma_T}{m_e c^3}, \tag{26}$$

where, L_s is the luminosity of the soft photons in the X-ray blob. EQPAIR considers the ratio of hard to soft compactness (l_h/l_s) and the soft compactness (l_s) as the parameters that will determine the temperature and the spectral index of the X-ray spectrum.

The (l_h/l_s) ratio: This is in effect equal to the ratio of L_{blob} over L_s and it determines the overall slope of the spectrum. If only inverse Compton scattering is important, models with the same l_h/l_s should have the same spectral slope. When $l_h/l_s \gg 1$, the source is said to be photon-starved and multiples orders of Compton scattering often contribute significantly to the equilibrium spectra, making them quite hard. On the other hand, the lower the l_h/l_s the steeper the spectrum will be.

Figure 10 shows spectra produced by EQPAIR for l_h/l_s=*1, 5, 10, 100* for l_s=*20*, τ_p=*0.5* and a soft photons black body input temperature of T_{bb}=*10eV*. The spectrum is given in units of *keV* cm^{-2} s^{-1}.

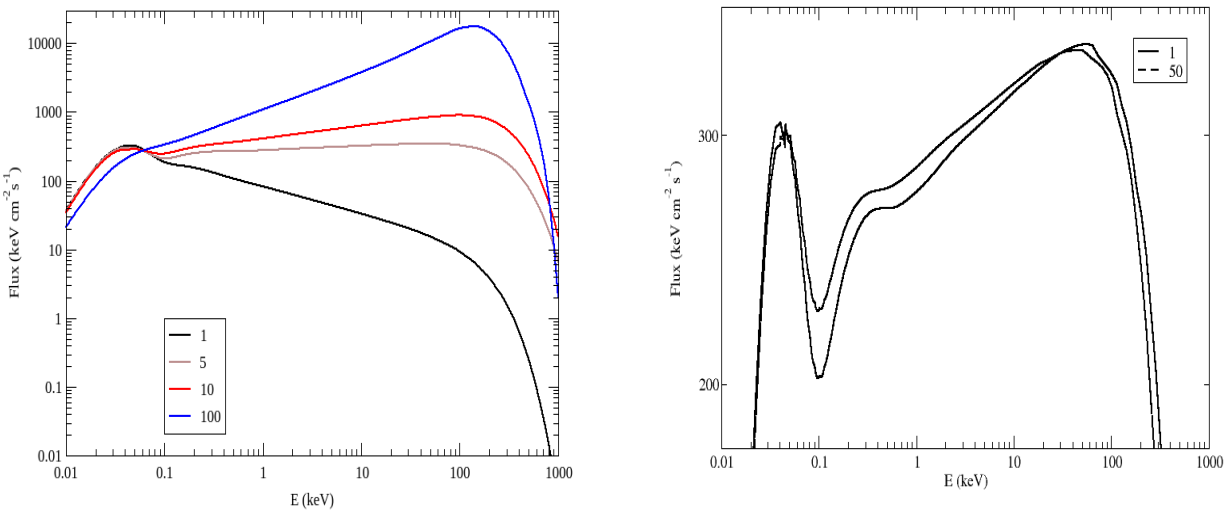

***Figure 10**: (Left-hand panel) Comptonization spectra produced by `EQPAIR` for l_h/l_s=1, 5, 10, 100. The other parameter are l_s=20, τ=0.5, T_{bb}=10eV. (Right-hand panel) `EQPAIR` Comptonization spectra for l_h/l_s=5, τ=0.5, kT_{bb}=10eV and l_s=1 (solid line) vs l_s=50 (dashed line).*

The left-hand panel of Fig. 10 shows that the spectrum hardens from a slope of -0.5 (for l_h/l_s=1) to +0.5 (when l_h/l_s=100). This occurs because as l_h/l_s increases, more and more power is supplied to the electrons, and they scatter the soft photons to higher energies. At the same time, the high energy cut-off (i.e. the temperature of the plasma electrons) decreases as we go from l_h/l_s=1 to l_h/l_s=100. This is because, as the soft photons scattered to higher energies, γ photons will be produced. They will interact with the softer photons and pairs will be created. So, as l_h/l_s increases, more and more pairs will be produced. In this case, the overall energy is distributed to more particles, hence the equilibrium temperature will decrease.

The soft photon compactness l_s: l_s determines the importance of photon-photon pair production. The compactness parameter is defined as the photon's luminosity over the size of the region. If $l_s \gg 1$ the source is "compact" and optically thick for the escaping gamma-rays. In this case, photon-photon production is important, and the temperature of the particles in the corona will be reduced. For $l_s \ll 1$ less pairs are produced and the particles in the corona should be hotter. In this case Coulomb cooling and Bremsstrahlung are more important compared to Compton cooling and the spectrum is altered at low energies.

Figure 10 (right panel) shows the Comptonization spectrum for l_s=1 (solid line) and l_s=50 (dashed line). The other parameters are l_h/l_s=5, τ=0.5, kT_{bb}=10eV. We observe a minor change of the slope and a decrease of the plasma temperature as l_s increases, due to the creation of γ-ray photons which leads to the creation of electron-positron pair, as we discussed.

It is relatively straight forward to estimate the X-ray compactness, but it is more complicated to estimate the soft photon compactness. In our case, the soft photons in the blob are those emitted by the disc directly below. The disc emits because it is hot due to the accretion process and due to the X-rays it will absorb, so:

$$L_s = L_{disc} + L_{Xabs}\,, \tag{27}$$

where L_{disc} is the luminosity of the soft photons due to the accretion heating while L_{Xabs} is the luminosity of the disc photons produced by the absorption of the X-rays emitted by the blob.

To estimate L_{disc}, we use the standard Shakura & Sunyaev (1973) theory to calculate the luminosity L_{ring} of a ring of width $2R_b$ at radius $R=10R_g$. We will then divide it by the surface of the ring (to get power per unit area) and we will multiply the result by the blob's area to get the disc luminosity that enters the blob (assuming that, due to its small height, only the disc photons emitted directly below the blob will enter into the X-ray corona).

According to Pringle (1981) the dissipation rate at distance R, per unit area per unit time is given by

$$D(R)=\frac{3GM\dot{M}}{4\pi R^3}\left[1-\left(\frac{R_{\text{in}}}{R}\right)^{1/2}\right]. \tag{28}$$

Therefore, the luminosity of the ring is,

$$\begin{aligned} L_{ring} &= \int_{R_d-R_b}^{R_d+R_b} D(R)\,2\pi R\,dR = \frac{3GM\dot{M}}{4\pi}\int_{R_d-R_b}^{R_d+R_b}\frac{1}{R^3}\left(1-\left(\frac{R_{\text{in}}}{R}\right)^{1/2}\right)2\pi R\,dR \\ &= \frac{3GM\dot{M}}{2R_g}\int_{9.981}^{10.019}\frac{1}{(r)^2}\left[1-\left(\frac{r_{\text{in}}}{r}\right)^{1/2}\right]dr, \end{aligned} \tag{29}$$

where $r=R/R_g$, and we used the fact that: $R_b=0.02R_g$ and $R_d=10R_g$. The constant outside the integral in the above equation is calculated as follows:

$\frac{3GM\dot{M}}{2R_g}=\frac{3G10^7M_\odot}{2R_g}\frac{L_{Edd}}{\varepsilon c^2}\left(\frac{M}{10^7M_\odot}\right)\left(\frac{\dot{M}}{\dot{M}_{Edd}}\right)$. Substituting Eddington's luminosity with $L_{Edd}=1.26\cdot10^{38}\left(\frac{M}{M_\odot}\right)erg/sec=1.26\cdot10^{38}\cdot10^7\left(\frac{M}{10^7M_\odot}\right)erg/sec$ then, for $\varepsilon=0.1$, $\left(\frac{M}{10^7M_\odot}\right)=1$, $\frac{\dot{M}}{\dot{M}_{Edd}}=0.055$, and $R_g=1.5\cdot10^{12}cm$, we get: $\frac{3GM\dot{M}}{2R_g}=10^{45}erg/sec$.

Finally,

$$L_{ring}=10^{45}erg/sec\int_{9.981}^{10.019}\frac{1}{(r)^2}\left[1-\left(\frac{r_{\text{in}}}{r}\right)^{1/2}\right]dr=9\cdot10^{40}erg/s, \tag{30}$$

and the disc luminosity from the area just below the X-ray source will be:

$$L_{disc}=0.5\frac{L_{ring}}{\pi(10.019^2-9.981^2)R_q^2}\pi R_b^2=4.2\cdot10^{37}erg/s. \tag{31}$$

The 0.5 factor is due to the fact that this luminosity will be emitted by the two surfaces of the disc.

Regarding L_{Xabs}, we assume that the X-ray source is emitting isotropically so, half of the X-ray photons will be emitted towards the disc (and the other half towards the observer). Out of this half another half will go directly under the blob in the case of a height-to-radius ratio of about unity for the X-ray blob. In other words, approximately *0.25* of L_h will be emitted directly below the blob. A fraction of the X-rays illuminating the disc will be reflected and the remaining will be absorbed. If we assume a cold, neutral gas, then roughly 25% of X-ray luminosity incident on the disc will be reflected, while the remaining *~75%* will be absorbed and will heat the disc. Therefore, $L_{Xabs}=0.25\cdot0.75\,L_h=0.19\,L_h$ and

$$L_s = L_{disc} + 0.19\, L_h \,. \tag{32}$$

By the definition of compactness, eq.(24), eq.(32) becomes,

$$l_s = \frac{L_s}{R_b}\frac{\sigma_T}{m_e c^3} = 0.02 + 0.19\, l_h \,. \tag{33}$$

3.3) The input soft spectrum

The disc spectrum can be approximated either by the XSPEC model diskbb or by the XSPEC model diskpn. The first gives the spectrum of an accretion disc, which consists of multiple blackbody components. The main parameter is the disc temperature at R_{in} (Mitsusa et al., 1984; Makishima et al., 1986). diskpn is an extension of diskbb model, including corrections for the temperature distribution near the blackhole. In this case the main model parameter is the maximum temperature of the disc (Gierlinski et al., 1999). In our work we chose the second option for the soft photons spectrum and we need to compute T_{max}.

For a geometrically-thin, optically thick, accretion disc around a Schwarzschild black hole and for the pseudo-Newtonial potential $\Phi(R) = -\frac{G M_{BH}}{R - 2R_g}$, the maximum disc temperature at $R > 9.5\, R_g$ is given by the following equation (Gierlinski et al., 1999):

$$T_{max} = c_0 f_{col} \left(\frac{3 \dot{M} q c^6}{8 \pi \sigma G^2 M_{BH}^2} \right)^{1/4} , \tag{34}$$

where $c_o = 0.1067$, $f_{col} = 1.7$, $q=1$, and σ is the Stefan-Boltzmann constant. In order to calculate T_{max} in our case, we express $\dot{M}$ and M_{BH} in terms of $\frac{\dot{M}}{\dot{M}_{Edd}}$ and $\frac{M_{BH}}{10^7 M_\odot}$. Using $\dot{M}_{Edd} = \frac{4\pi G M m_p}{\varepsilon c \sigma_T}$ eq.(34) becomes,

$$T_{max} = c_0 f_{col} \left(\frac{3 q c^6}{8 \pi \sigma G^2} \right)^{1/4} \left(\frac{\dot{M}}{\dot{M}_{Edd}} \right)^{1/4} (\dot{M}_{Edd})^{1/4} \left(\frac{M_{BH}}{10^7 M_\odot} \right)^{-1/2} (10^7 M_\odot)^{-1/2} =$$

$$= c_0 f_{col} \left(\frac{3 q c^6}{8 \pi \sigma G^2} \right)^{1/4} \left(\frac{4 \pi G M_{BH} m_p}{\varepsilon c \sigma_T} \right)^{1/4} (10^7 M_\odot)^{-1/2} \left(\frac{M_{BH}}{10^7 M_\odot} \right)^{-1/2} \left(\frac{\dot{M}}{\dot{M}_{Edd}} \right)^{1/4} =$$

$$= c_0 f_{col} \left(\frac{3 q c^5 m_p}{2 \sigma G 10^7 M_\odot \varepsilon \sigma_T} \right)^{1/4} \left(\frac{M_{BH}}{10^7 M_\odot} \right)^{-1/4} \left(\frac{\dot{M}}{\dot{M}_{Edd}} \right)^{1/4} =$$

$$= 29 \left(\frac{M_{BH}}{10^7 M_\odot} \right)^{-1/4} \left(\frac{\dot{M}}{\dot{M}_{Edd}} \right)^{1/4} eV = 14\, eV \,,$$

for $M_{BH} = 10^7 M_\odot$ and $\dot{M} = 0.055\, \dot{M}_{Edd}$.

3.4) The optical depth

The Thompson optical depth τ_p is another parameter of EQPAIR. It is measured from the center to the surface of the scattering region. For a purely thermal plasma with no pair production only electrons produce the thermal Comptonization spectrum with optical depth equal to τ_p. When pairs are produced the total optical depth is larger than τ_p and it is estimated self-consistently by the code. In our computations we assumed $\tau_p = 1$.

Figure 11 shows how the Comptonization spectrum changes for different values of τ_p. The parameters of the model in this plots are $l_h/l_s=5$, $l_s=20$, $T_{bb}=10eV$ and $\tau_p=0.3, 0.5, 1, 2, 5$. The slope of the spectrum does not change significantly but the temperature, kT_e, decreases when τ_p increases. The reason of this is as follows. When the region is optically thick more electron-photon interaction (inverse Compton scattering) occur and as the soft photons scattered to higher energies, γ photons will be produced. They will interact with the softer photons and pairs will be created. As a result the temperature kT_e decreases when pairs produced as we have discuss earlier.

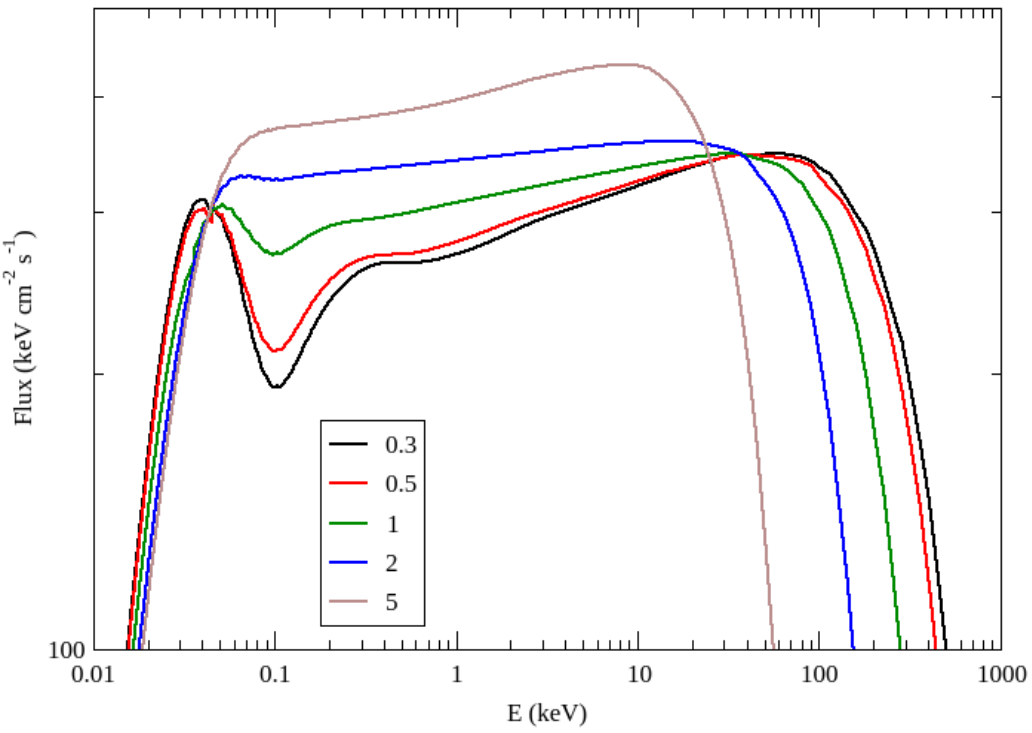

Figure 11: *EQPAIR comptinization spectra for τ=0.3, 0.5, 1, 2, 5 and l_h/l_s=5, l_s=20 and T_{bb}=10eV.*

CHAPTER 4: Results & Conclusions

4.1) The dissipation profile for X-ray photons

Let us consider the case when the X-ray producing blob appears. According to what we discussed in Section 3.2, the power deposited to the blob initially, $L_{h_{init}}$, will be equal to L_{blob}, given by eq.(23). Then, according to Haardt et al. (1994), the power transferred to the blob will decrease exponentially with a discharge timescale, t_d. This is the timescale that controls the heating of the particles, and is proportional to the blob light crossing time:

$$t_d = \alpha\left(\frac{R_b}{c}\right). \tag{35}$$

The proportionality constant, α, is the same with the constant in eq.(22). So, adopting $\alpha = 10$ and using eq.(21) for R_b, the above equation becomes:

$$t_d = \alpha\left(\frac{R_b}{c}\right) = 10\left(\frac{3\cdot 10^{10}\, cm}{3\cdot 10^{10}\, cm/s}\right) = 10\, s\,. \tag{36}$$

So, we assume the following profile for L_h as a function of time:

$$L_h(t) = L_{blob}\exp(-t/t_d)\,. \tag{37}$$

By substituting L_{blob} and t_d from eq.(23) and eq.(36), the above equation becomes,

$$L_h(t) = 3\cdot 10^{41}\exp(-t/10\,s)\, erg/s\,. \tag{38}$$

Applying the definition of compactness (see eq.24), the hard compactness can then be parameterized as

$$l_h(t) = 285\exp(-t/10\,s)\,. \tag{39}$$

Figure 12 shows how the X-ray compactness and luminosity change with time (solid line in the left and right panel, respectively). The luminosity plotted in this figure is the observed one, which is $L_h/2$, because half of the luminosity is emitted towards the accretion disc (if X-rays are emitted isotopically). The figure shows that L_h (and l_h), stay roughly constant fin the beginning, up to *1-3s*, and then they decrease exponentially. The horizontal line in the right panel indicates the luminosity level of 10^{41} *erg/s*. For typical AGNs, we would need more than 10 blobs to be active for the X-ray luminosity to be more than $10^{42}\ erg/s$, on average, as observed.

As for l_s, using eq.(33) we get:

$$l_s(t) = 0.02 + 0.19\cdot 285\exp(-t/10\,s) = 0.02 + 54.15\exp(-t/10\,s)\,. \tag{40}$$

The dashed line on the left panel of Fig. 12 shows $l_s(t)$ and the dot-dashed line show the ratio l_h/l_s. This ratio stays constant at a value of ~4, and then decreases. This is because, the main source of heating for the disc directly below the blob is the X-rays that are absorbed. Therefore, the soft photons compactness follows the X-ray compactness. But, at later times, the X-ray heating decreases enough so that the soft photons emitted by the disc below the blob are those due to the disc heating by the accretion process. After that, l_s remains constant at a value of $l_s \simeq 0.02$ while l_h still decreases. It is around that time that the ratio l_h/l_s starts decreasing exponentially.

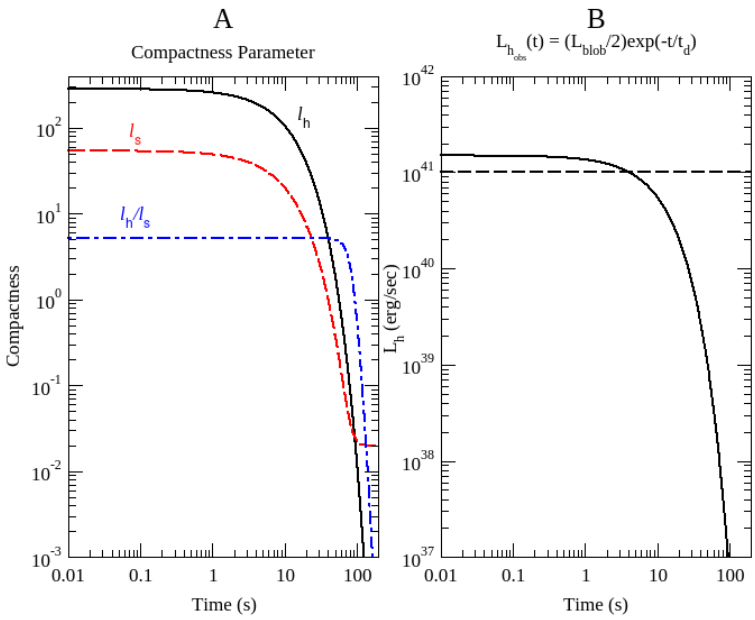

***Figure 12**: (Panel A) Plot of l_h, l_s and l_h/l_s as a function of time (solid, dashed, dot-dashed line respectively). (Panel B) Plot of L_h that an observer will detect as a function of time.*

4.2) The variable spectrum of the X-ray corona

We used the l_h/l_s and the l_s values plotted in Fig. 12 from 0.01s to 100s, and we run `EQPAIR` 10000 times (with a logarithmic spacing in time) to study how the blob spectrum changes in time. Each time we kept the other model parameters fixed to the values we discussed in the previous Chapter (i.e. $\tau_p=1$, and $T_{bb}=14eV$).

Figure 13 shows the spectrum at the times listed in the first column of Table 1. Using a power-law with an exponential cut-off model, we estimated the spectral slope Γ[3], the high energy cut-off, E_{cut}, and the flux in the *2-10keV* band. The results are listed in the second, third and forth column of Table 1.

t (*s*)	Γ	E_{cut} (*keV*)	Flux (2-10keV) (10^{-14} *erg cm^{-2} s^{-1}*)
0.01	1.95	500	6.34
10	1.95	500	6.34
30	1.96	500	6.30
50	1.97	480	6.01
60	1.99	450	5.52
70	2.03	400	4.46
80	2.14	-	2.73

Table 1: The spectrum slope Γ, high-energy cut off, E_{cut}, and the 2-10keV flux of the corona spectrum at different times.

3 Γ is the slope of the spectrum in units of *photons s^{-1} cm^{-2} keV^{-1}*.

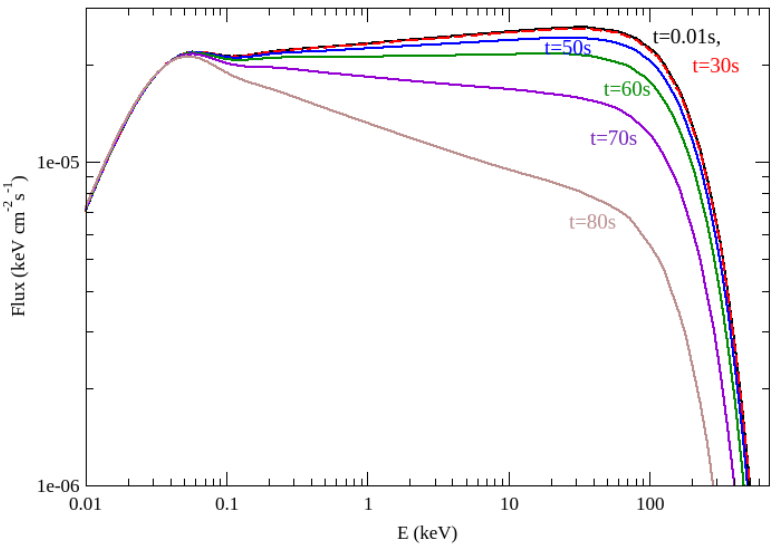

***Figure 13**: The spectral evolution of the source. Each solid line represent the source spectrum at a certain time.*

Both the spectra plotted in Fig. 13 and the values listed in Table 1 show that, initially, the spectral slope Γ is ~2. The slope remains roughly the constant as long as l_h/l_s also remains constant, and then the spectrum steepers as l_h/l_s starts decreasing. In fact, for most of time, the spectral slope is around 1.95-2, which is almost identical to the average slope of the Type 1 AGN, as we mentioned in the Introduction (see 1.3.1).

Due to the fact that L_h decreases with time, the overall normalization of the spectrum also decreases. As a result the flux in the *2-10 keV* band decreases as well. In the left panel of Fig. 14 we plot the spectral slope Γ as a function of the *2-10 keV* flux. Based on what we said above, the figure shows that the spectrum softens (the slope steepens) as the flux decreases. This is opposite to what we observe in AGN (see 1.3.2).

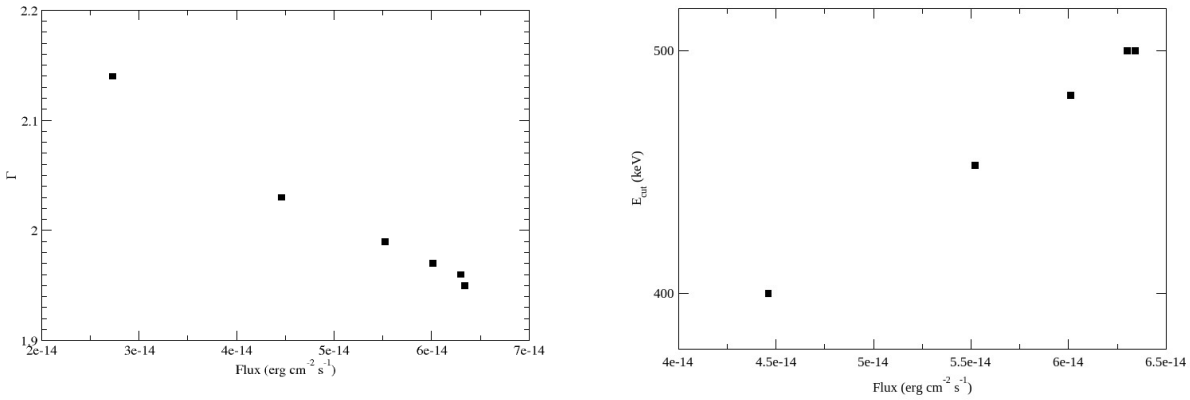

***Figure 14**: (Left-hand Panel) Plot of the spectral slope Γ as a function of the 2-10keV flux. As the flux increases, the spectrum is getting harder. (Right-hand Panel) Plot of the cut-off energy (plasma temperature) as a function of 2-10keV flux.*

The cut-off energy for our simulations is at *400-500keV* range which is higher than the average observed values of *100-200keV* (see 1.3.1). Therefore, the model predicts a "hotter" X-ray source than what we observe. The reason of this difference might be relativistic effects (such as gravitational redshift) that may affect the observed X-ray source temperature. Tamborra et al. (2018) have studied the importance of GR effects on the high energy cut-off in AGN. They found that for a corona distributed in the inner disc, up to a distance of $R=10R_g$, the ratio of the intrinsic to the observed cut-off energy is of the order of ~1.3, for systems that we observe almost face-on. This would imply a range of the observed E_{cut} between *380 - 300 keV*, which is still higher than what has been measured from observations.

The third column of Table 1, shows how E_{cut} evolves with time. The cut-off energy stays constant (up to ~30s) and then decreases. This can be explained by eq.(38) which show the L_h evolution. After a few times the t_d, the timescale of L_h evolution, L_h has been decreased and the power injected into the blob has been significantly reduced. Therefore less power is supplied to the corona electrons and the temperature, kT_e, also decreases.

Figure 15 shows the flux in 6 energy band, namely *0.5-1*, *1-2*, *2-4*, *4-7*, *7-10* and *10-20 keV*, as a function of time. These fluxes were estimated from the 10000 `EQPAIR` spectra that we computed as explained above. These curves show the temporal evolution of the source flux in various energy bands.

The flux in all energy bands stays roughly constant up to 60s but then decreases quickly. The right panel of Fig. 15 (left panel) shows the same fluxes but normalized to their maximum flux. The higher energy band (*10-20 keV*) seems to decline first and then the softer energy bands follow. The logic behind this behavior is that in later time the slope steepens and the flux in the hard energy bands decrees more (see Table 1 and Fig. 13). However this effect would imply that variations are delayed in the soft band. We would see first the flux varying in the high and then in the lower energy band, which is not in agreement with the observations (see 1.3.3).

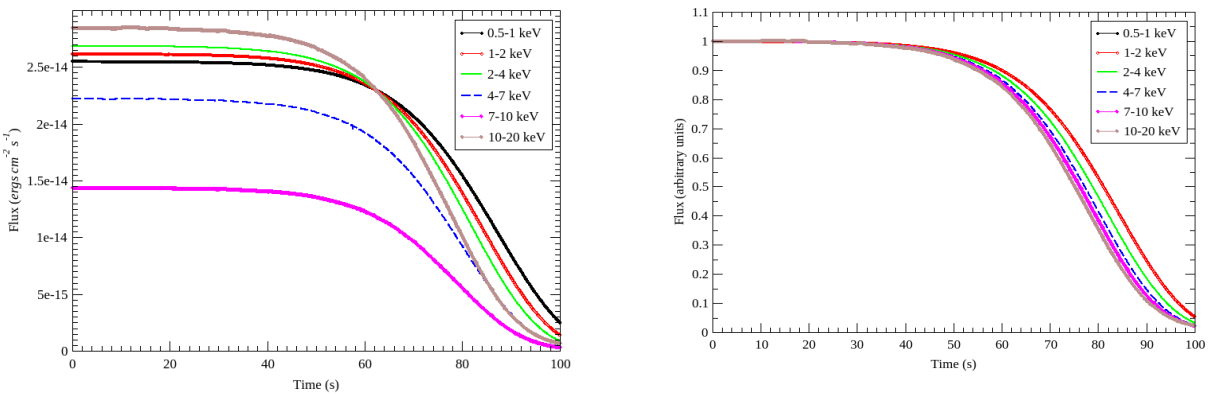

***Figure 15**: The temporal evolution of the source flux in 0.5-1, 1-2, 2-4, 4-7, 7-10 and 10-20 keV energy bands estimated from 10000 EQPAIR spectra. Right-hand panel is the same to left-hand panel but normalized to their maximum flux.*

4.3) Conclusions

In this work we studied the GRV model, which has been proposed to explain the X-ray variability in AGN. In particular, we examined the model version proposed by Haardt et al. (1994). In this model a fraction of the accretion power is stored in the magnetic field and then this energy is released and heats electrons in a small region. Low energy soft photons emitted by the disc enter the corona, they are interacting with the particles by Inverse Compton scattering and then, they are up-scattered to higher energies. To study this, we calculated the size and total luminosity of a single blob at a distance of 10Rg as well as the luminosity of the soft photons that will be Comptonized (Chapter 3). We assumed that the power released by the blobs follows an exponential decay with a discharge timescale proportional to the blob's light-crossing time (Chapter 4). Using the comptonization code `EQPAIR`, we determined the time evolution of the emitted X-ray spectrum and we calculated the flux in 6 different energy bands (Chapter 4).

The parameter that determines the importance of Inverse Compton scattering and consequently how much the spectral shape of the soft photons will be altered, is the Compton parameter y (Chapter 2). In order for the Comptonization process to be important, the Compton parameter should be $y \gg 1$. As we have discussed in Section 2.2, y is depends on the mean electrons' temperature and the optical depth of the scattering region, kT_e and τ, respectively. `EQPAIR`, does not consider kT_e as a parameter because the plasma temperature is calculated self-consistently by the code, based on the ratio of the X-ray to soft photons luminosity and on the soft photons compactness. This is a dimensionless parameter which depends on the ratio of the photon's luminosity over the scattering region size. This parameter determines the "optical depth" of the soft photons to photon-photon interactions. The larger it is (i.e. the more compact the source will be), the more frequently γ-ray photons will interact with soft photons and pairs will be produced. In this case the available power will be distributed to more particles and the temperature will decrease. The code also considers the disc blackbody spectrum and the electron optical depth, τ_p, in the scattering region. When e^-, e^+ pairs are created the total optical depth is higher than τ_p, and is calculated by the code.

Our main results are as follows:

- For most of the time the spectral slope Γ is around 1.95-2 which matches the observations for the average value of Γ for Type 1 AGNs. However, as the flux in 2-10keV energy band decreases, the slope steepens (Γ increases) which is different from what the observations show. The reason of this behavior is as follows: the value of l_h/l_s determines the spectral slope. In our case, l_s reaches a constant value for large t and l_h decreases exponentially. Thus, l_h/l_s also decreases making the slope "softer" as we have discussed in Chapter 3. At the same time, the decrease in the power that heats the electrons decreases, hence the "softer when fainter behavior". We suspect that, any model that assumes a constant soft photon's compactness and the X-ray luminosity decreases exponentially with time, the spectral slope will always become steeper with decreasing flux, which is not in comparison with the observational results.

- The intrinsic spectral high energy cut-off is *~400-500keV* which is higher than the observed values in the energy spectra of a few AGN. When we consider GR effects, the observed values are expected to be smaller by a factor of ~1.3, but the difference between the model predicted and the observed values still remains.

- The cut-off energy stays constant at *500keV* up to 30s (see Table 1) and then decreases due to the fact that L_h decreases and less power is supplied to the electrons. We observe a weak linear relation between $log(E_{cut})$ and the flux of the *2-10keV* band. As the flux decreases the cut-off energy decreases. If this behavior of the model is correct, then we should observe a

similar behavior when we examine many objects with different luminosities and E_{cut}. However, observations show no relation between E_{cut} and the luminosity (see Tortosa et al., 2018). However, the relation we found is weak and, even if it were present, perhaps we could not observe it.

- We studied the flux variations in various energy bands, from 0.5-*1keV* to *10-20keV*. The flux in the higher energy bands (i.e. *7-10keV* and *10-20keV*) decreases faster than the flux in the softer bands (i.e. *0.5-1keV* or *1-2keV*). This would imply that the observed variations in the soft band should be delayed with respect to the variations at higher energy bands. However, the observational results show a delay of the softer band with respect to the variations in the higher energy band.

Overall, some of the model's predictions are consistent with the observations, but, the spectral slope, Γ, appears to decrease when flux decreases which is is opposite to what we observe in AGN. Furthermore, the value of Ecut is much higher than the value we observe and the flux of the soft bands decreases slower than the flux in the hard bands, which is also in conflict with the observed data.

We therefore conclude that the Haardt et al. (1994) version of the GRV model does not match the observations and therefore is not accepted as an explanation of the X-ray variability in AGNs.

References

Coppi P. S. "EQPAIR: Modeling the Emission from a Hybrid Thermal/Non-Thermal Plasma." 2002.

Galeev A. A., Rosner R., & Vaiana G. S., 1979, ApJ, 229, 318.

Gierlinski, M., Zdziarski A. A., Poutanen J., Coppi P. S., Ebisawa K. & Johnson W. N., 1999, MNRAS, 309, 496.

Haardt F., Maraschi L. & Ghisellini G., 1994, ApJ, 432, L95.

Longair M. S. *High Energy Astrophysics*. Cambridge: Cambridge University Press, 2017.

Lusso E. et al., 2012, MNRAS, 425, 623.

Papadakis I. E. & Lawrence A., MNRAS, 272, 161.

Petrucci P.-O. et al., 2013, A&A, 549, 17.

Pozdnyakov L. A., Sobol I. M. & Syunyaev R. A., 1983, ASPRv, 2, 189.

Pringle J. E., 1981, ARAA, 19, 137.

Ricci C. et al., 2017, ApJ, 233, 38.

Rosswog S. & Brüggen M. *Introduction to High-energy Astrophysics*. Cambridge: Cambridge University Press, 2007.

Rybicki G. B. & Lightman A.P. *Radiative Processes in Astrophysics*. Wiley: New York, 1979.

Shakura N. I., & Sunyaev R. A., 1973, A&A, 55, 155.

Sobolewska M. A. & Papadakis I. E., 2009, MNRAS, 399, 1597.

Svensson R. & Zdziarski A.A., 1994, ApJ, 436, 599.

Tamborra F., Papadakis I.E., Dovčiak M. & Svoboda J., 2017, MNRAS, 475, 2045

Tortosa A., Bianchi S., Marinucci A., Matt G. & Petrucci P. O., 2018, A&A, 614, 9.